Article

H2 Evolution from a Thiolate-Bound Ni(III) Hydride

Nina X. Gu, Paul H. Oyala, and Jonas C. Peters

J. Am. Chem. Soc., **Just Accepted Manuscript** • Publication Date (Web): 04 Apr 2020

H_2 Evolution from a Thiolate-Bound Ni(III) Hydride

Nina X. Gu, Paul H. Oyala, and Jonas C. Peters*

Division of Chemistry and Chemical Engineering, California Institute of Technology, Pasadena, California 91125, United States

Supporting Information Placeholder

ABSTRACT: Terminal Ni^{III} hydrides are proposed intermediates in proton reduction catalyzed by both molecular electrocatalysts and metalloenzymes, but well-defined examples of paramagnetic nickel hydride complexes are largely limited to bridging hydrides. Herein, we report the synthesis of an $S = ½$, terminally bound thiolate-Ni^{III}-H complex. This species, and its terminal hydride ligand in particular, have been thoroughly characterized by vibrational and EPR techniques, including pulse EPR studies. Corresponding DFT calculations suggest appreciable spin leakage onto the thiolate ligand. The hyperfine coupling to the terminal hydride ligand of the thiolate-Ni^{III}-H species is comparable to that of the hydride ligand proposed for the Ni-C hydrogenase intermediate (Ni^{III}-*H*-Fe^{II}). Upon warming, the featured thiolate-Ni^{III}-H species undergoes bimolecular reductive elimination of H_2. Associated kinetic studies are discussed and compared with a structurally related Fe^{III}-H species that has been recently reported to also undergo bimolecular H-H coupling.

INTRODUCTION

Hydrogen is a promising alternative to carbon-based fuel, and homogenous electrocatalysts for the H_2 evolution reaction (HER) have been scrutinized for possible practical applications and especially as well-defined systems for mechanistic studies.[1] Although metal hydrides may not be required intermediates of HER,[2] terminally bound Ni^{III} hydride intermediates have been implicated in both stoichiometric[3] and catalytic[4] proton reduction[5] mediated by Ni-based systems. Additionally, paramagnetic Ni^{III} hydride intermediates have been proposed in enzymatic H_2 evolution (Fig. 1, top). A bridging hydride has been identified in the $S = ½$ [NiFe] hydrogenase intermediate (Ni^{III}-H-Fe^{II}) assigned as the Ni-C state,[6] and computational data suggest that the hydride is bound more tightly to Ni than to Fe (Ni-H: 1.61 Å, Fe-H: 1.72 Å).[7,8] Additionally, EPR data support an estimated Ni-H bond length of ~1.6 Å.[6a] The possible role of a [NiFe] hydrogenase state featuring a terminal Ni^{III}-H has also been computationally investigated for the related case of H_2 oxidation.[9] Furthermore, studies on Ni-substituted rubredoxin, a model enzyme for [NiFe] hydrogenase bearing a single Ni center in the active site, support the intermediacy of a terminal Ni^{III}-H species in proton reduction catalysis.[10]

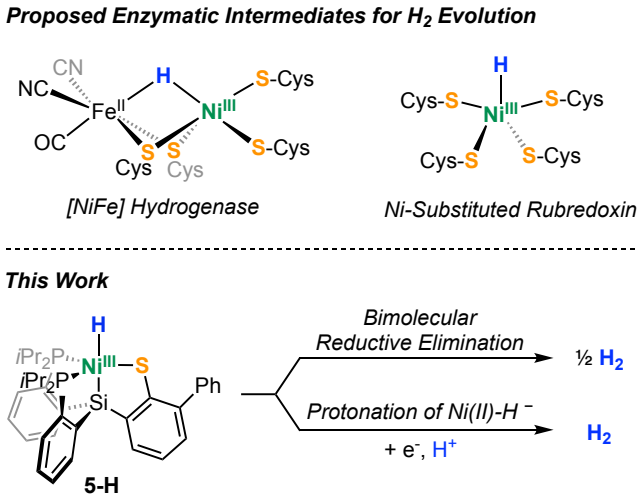

Figure 1. (top) Proposed hydrogenase intermediates featuring a Ni^{III} hydride motif (bottom) Accessible pathways for H_2 evolution from the Ni hydride complexes described in this work.

Owing to their posited role as intermediates in HER catalysis, well-characterized paramagnetic nickel hydride model complexes are needed for detailed study, but examples are lacking, whereas examples of related terminally bound $Ni^{I/III}$-Me species are available.[11] For hydride cases, such species largely feature bridging hydrides bound to two metal centers (Ni-H-Ni),[12] three metal centers (Ni_3-(H)),[12d,13] or as borohydride adducts (Ni-H-BR_3).[14] Characterization data for *terminally* bound $Ni^{I/III}$ hydride complexes are scant. In previous work, irradiation of a matrix-isolated sample containing $Ni(CO)_4$ and HI yielded several EPR-active compounds, including a species assigned as H-$Ni^{I}(CO)_4$.[15] Related solid-state experiments employing $Ni(CN)_4^{2-}$ generated a $[H\text{-}Ni(CN)_n]^x$ species as one of the EPR-active prod-

ucts.[16] Additionally, the Ni^{III} hydride $[(PS_3)Ni^{III}H][PPN]$ has been reported in solution by treatment of the analogous Ni^{III}-OPh complex with pinacolborane.[17,18] Characterization data for this species was limited; in particular, the inferred hydride ligand was not confirmed by spectroscopic analysis (*vide infra*).

Herein, we generate and spectroscopically characterize a thiolate-supported, terminally-bound Ni^{III}-H species at low temperature. Direct identification of the terminal hydride ligand is confirmed by both vibrational and pulse EPR data. Of note, bimolecular reductive elimination of H_2 proceeds upon warming this Ni^{III}-H species, followed with N_2 binding to quantitatively generate a Ni^{II}-N_2 product. Stoichiometric reactivity studies from the Ni^{II}-H^- and Ni^{III}-H species featured herein demonstrate the viability of both a heterolytic and homolytic pathway for H_2 evolution.

RESULTS AND DISCUSSION

Synthesis and characterization of Ni precursors.

Following a recent study of a ferric Fe(H)(N_2) species featuring a tetradentate bis(phosphine)(silyl)(thiolate) ligand (Scheme 1),[19] we targeted the generation of a trivalent Ni-H species supported by this ligand framework. Treatment of $HSiP_2S^{iPr}$ (**1**)[19] with $Ni(COD)_2$ (COD = 1,5-cyclooctadiene) yields a thioether-bound Ni(II) hydride, $(SiP_2S^{iPr})Ni^{II}H$ (**2**, Scheme 1a; see Fig. 2A for solid-state structure) with a Ni-H stretch at 1737 cm^{-1} and a ^1H NMR hydride signal at -6.90 ppm (t, $^2J_{H,P}$ = 46.3 Hz, in C_6D_6). Addition of KC_8 to **2** results in the reductive cleavage of the S-*i*Pr bond to furnish a thiolate-bound Ni(II) hydride, $[(SiP_2S)Ni^{II}H]K$ (**3**, see Fig. 2B for solid-state structure; ν(Ni-H) at 1677 cm^{-1}; hydridic resonance at -8.10 ppm (t, $^2J_{H,P}$ = 43.0 Hz) in C_6D_6).

Protonation of hydride **3** with $[H(OEt_2)_2][BAr^F{}_4]$ under an N_2 atmosphere affords a nickel(II) complex, $(SiP_2S)Ni^{II}(N_2)$ (**4**), which crystallizes as the dimeric, dinitrogen-bridged species, $[(SiP_2S)Ni^{II}]_2(N_2)$ (**4'**) (Scheme 1B). XRD data confirms the structure of **4'** (Fig. 2C; Table 1) and reveals an N-N bond length of 1.115(2) Å. Solid-state IR data of crystals of **4'** do not show an N_2 stretch, consistent with the inversion center gleaned in the solid-state structure. However, an intense N_2 stretch at 2200 cm^{-1} is observed in solution under an N_2 atmosphere, indicating that **4'** dissociates to monomeric **4** in solution. Notably, a solid thin-film produced by concentration of a solution of **4** under an N_2 stream does not exhibit the N_2 stretch at 2200 cm^{-1}, demonstrating that **4'** predominates upon concentration and is consistent with an equilibrium between **4** and **4'**.

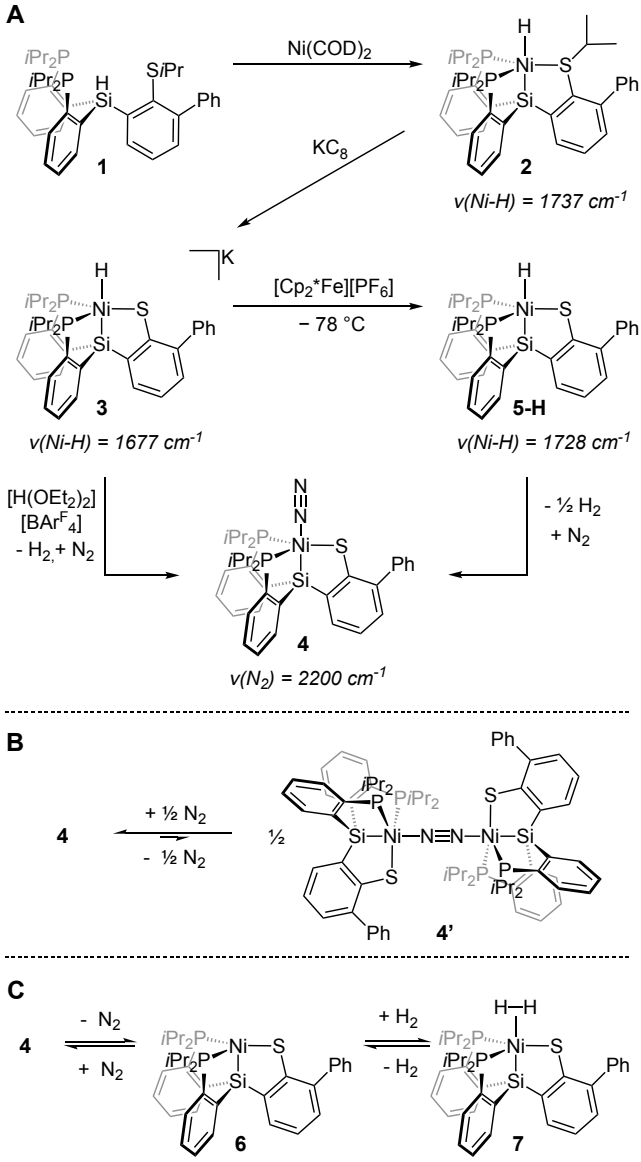

Scheme 1. Synthesis and numbering scheme of compounds discussed herein.

A degassed solution of diamagnetic **4** bears NMR features distinct from those acquired under an N_2 atmosphere, intimating the loss of N_2 to generate a diamagnetic four-coordinate Ni species, $(SiP_2S)Ni^{II}$ (**6**), under vacuum (Scheme 1C). Exposure of **6** to an atmosphere of H_2 yields the five-coordinate Ni^{II}-H_2 complex, $(SiP_2S)Ni^{II}(H_2)$ (**7**). XRD data obtained on crystals grown under an atmosphere of H_2 are consistent with the assignment of **7** (Fig. 2D). In particular, the structural similarity between **7** and **4'** suggests that **7** bears an intact H-H fragment in the solid state, which disfavors alternative assignments as the $Ni(H)_2$ or NiH(SH) species in the solid state (Table 1). While the H_2 unit could not be reliably identified from the XRD data, positive residual electron density located trans to the silyl group is consistent with a bound H_2 ligand (Fig. 2E), as has been previously observed in XRD data of related H_2-bound complexes.[20] Additionally, the HD analogue, $(SiP_2S)Ni^{II}(HD)$, exhibits a $^1J_{HD}$ of 35 Hz (toluene-d_8,

−80 °C), indicative of an intact dihydrogen unit in solution.[21] Examples of Ni(H_2) complexes are rare,[22,23] and **7** is distinct by virtue of the thiolate donor ligand; H_2 activation across a Ni-thiolate bond has been invoked elsewhere.[24]

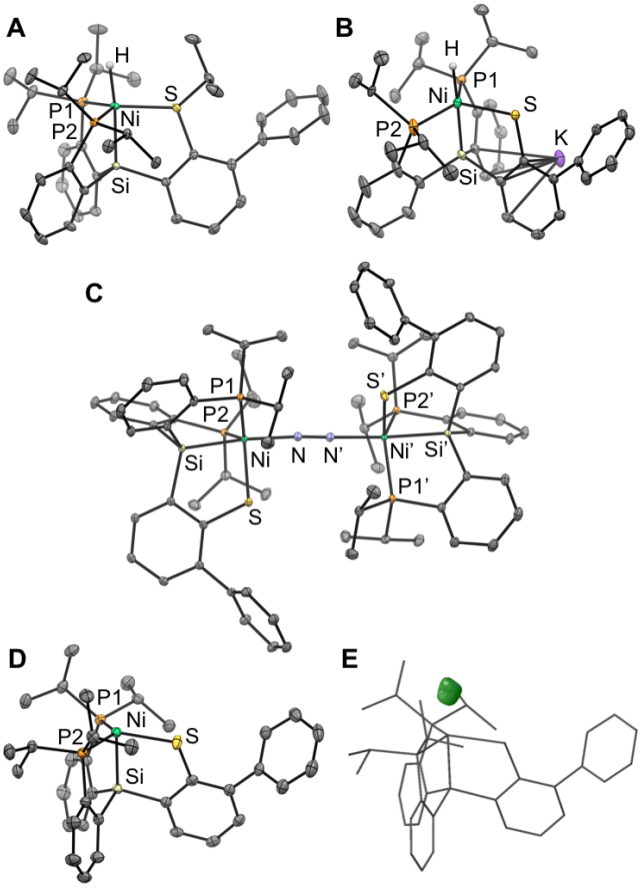

Figure 2. X-ray structures of **2** (A), **3** (B), **4'** (C), **7** (D), and the residual positive electron density plot of **7** (isovalue: 0.78) (E). C-*H* hydrogen atoms and solvent molecules are omitted for clarity. Ellipsoids are depicted at 50% probability.

Table 1. Bond lengths of 4' and 7.

	d(Ni-S)	*d*(Ni-P)	∠(P-Ni-P)	∠(P-Ni-S)
4'	2.3320(6)	2.2405(5)	129.82(3)	109.69(2)
		2.2627(6)		116.49(2)
7	2.3089(9)	2.208(1)	129.12(4)	108.62(4)
		2.2246(9)		119.77(4)

Generation and characterization of a Ni^{III}-H.

The cyclic voltammogram of **4** in THF reveals a reduction event at −2.33 V vs. Cp_2Fe/Cp_2Fe^+, and **4** slowly catalyzes HER in the presence of PhOH as a weak acid source at a strongly cathodic potential (see Supporting Information for details).[25] Treatment of the Ni^{II}-H^- **3** with PhOH in THF results in quantitative generation of H_2 and (SiP_2S)NiOPh$^-$, demonstrating a heterolytic pathway for H-H bond formation within the system. For comparison, we also explored the viability of a homolytic pathway for H_2 generation from the corresponding Ni^{III}-H species. Examples of $M^{n/n+1}$ hydride pairs that can access H_2 evolution via a homolytic pathway from one oxidation state and a heterolytic pathway from another are rare.[27e,28a] Whereas protonation of a metal hydride complex to release H_2 is commonly observed,[1,26] examples of bimolecular reductive elimination of H_2 from two well-defined M-H units is less precedented,[19,27,28,29] although such a pathway has been proposed in a number of HER electrocatalysts.[1,4f,27e,30]

The cyclic voltammogram of the Ni^{II}-H^- species **3** exhibits a reversible feature at −1.26 V vs. Cp_2Fe/Cp_2Fe^+ in THF that corresponds to the formal $Ni^{II/III}$ couple, and chemical oxidation using [Cp*$_2$Fe][PF_6] at −78 °C in THF yields a dark blue-green solution of the desired (SiP_2S)Ni^{III}H (**5-H**) species. Solutions of **5-H** are thermally sensitive (*vide infra*) and were therefore handled at low temperatures to obtain spectroscopic data. As expected for a Kramer's doublet species, **5-H** exhibits paramagnetically shifted peaks in its ^{1}H NMR spectrum (THF-d_8, −40 °C). A characteristic terminal Ni-H stretch is observed in the IR spectrum at 1728 cm^{-1} (THF solution, −78 °C) that vanishes upon deuteration via the analogue (SiP_2S)Ni^{III}D (**5-D**).[31] This Ni-H stretch is in good agreement with the DFT-predicted gas-phase value of 1720 cm^{-1}.[32]

The 77 K X-band CW EPR spectrum of **5-H** confirms the expected S = ½ spin state (Fig. 3) and is simulated with a rhombic g tensor of **g** = [2.166, 2.056, 2.039] and hyperfine coupling to two equivalent ^{31}P nuclei (**A**(^{31}Pα) = **A**(^{31}Pβ) = ±[200, 210, 260] MHz) and a Ni-*H* nucleus (**A**(^{1}H) = ±[1.63, 1.63, 31.9] MHz; for **5-D**, **A**(^{2}H) = ±[0.25, 0.25, 4.9] MHz). These simulation parameters are consistent with Q-band ^{1}H, ^{31}P Davies ENDOR and ^{2}H HYSCORE data for **5-H** and **5-D** (see Supporting Information). Notably, the ^{1}H dipolar tensor (**T**) of **5-H** is axially symmetric (**A**(^{1}H) = a_{iso} + **T**; **T** = ±[-10.1, -10.1, 20.2] MHz), as can be anticipated for a terminally bound metal hydride (M−H), whereas a rhombic dipolar tensor would instead be expected for an approximately symmetric bridging hydride (M−H−M).[33] By scaling the isotropic component of the ^{1}H hyperfine coupling tensor (|a_{iso}(^{1}H)| = 11.7 MHz) by the a_{iso} value for a hydrogen atom (1420 MHz),[34] spin density localized at the hydride is estimated as ±0.008 e$^-$. The DFT-optimized structure in the gas phase for **5-H** (M06l) predicts a Mulliken spin density of -0.005 e$^-$ on the hydride, consistent with the experimental data.

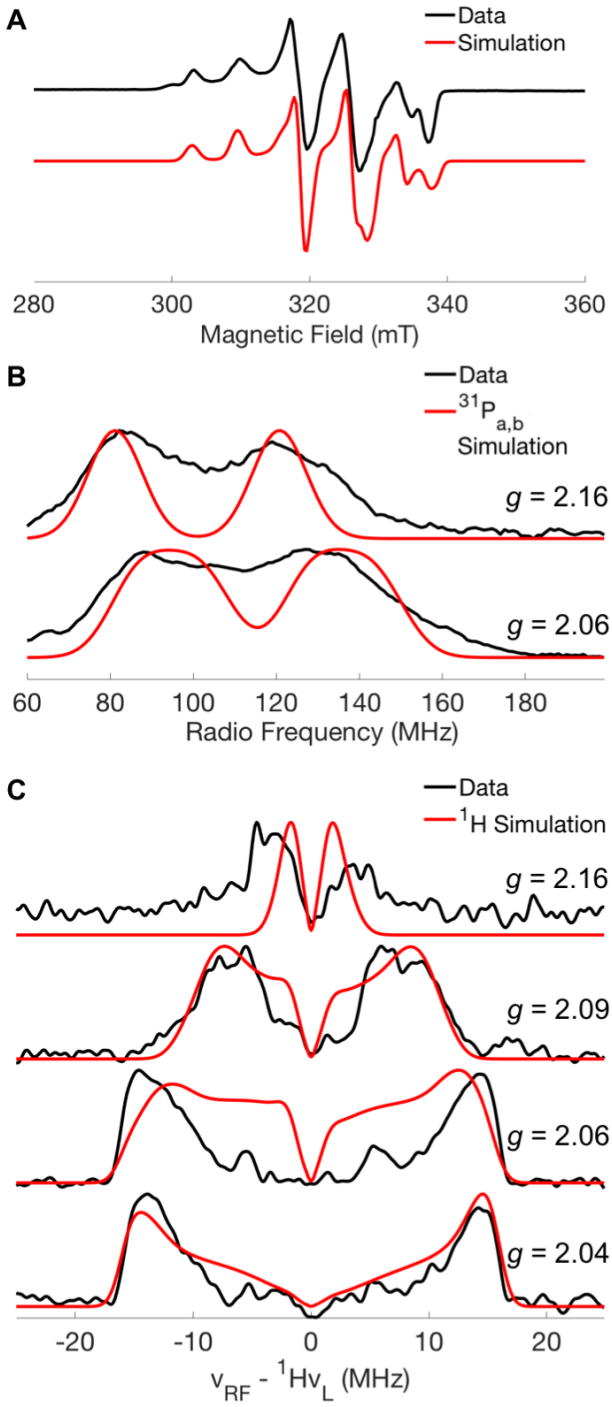

Figure 3. (a) X-band CW EPR spectrum of **5-H** in 2-MeTHF with simulation. Simulation parameters: **g** = [2.166, 2.056, 2.039]; **A**(^{31}Pα) = **A**(^{31}Pβ) = [200, 210, 260] MHz); **A**(^{1}H) = [1.6, 1.6, 31.9] MHz.; Acquisition parameters: MW frequency = 9.371 GHz; temperature = 77 K; MW power = 2 mW; modulation amplitude = 2 G; conversion time = 82 ms. (b) Field-dependent ^{31}P Q-band Davies ENDOR spectra of **5-D**. (c) Field-dependent Q-band Davies ENDOR ^{1}H minus ^{2}H difference spectra of **5-H** and **5-D**; difference spectra were smoothed using a 5-point Savitzky-Golay filter. ENDOR samples were prepared in 2-MeTHF, and spectra are simulated with the same g-values and hyperfine coupling as Fig. 3A. Experimental conditions for Fig. 3B, 3C: microwave frequency = 34.040 GHz; MW π pulse length = 80 ns; interpulse delay τ = 400 ns; π_{RF} pulse length = 15 μs; T_{RF} delay = 2 μs; shot repetition time (srt) = 2 ms; temperature = 12 K.

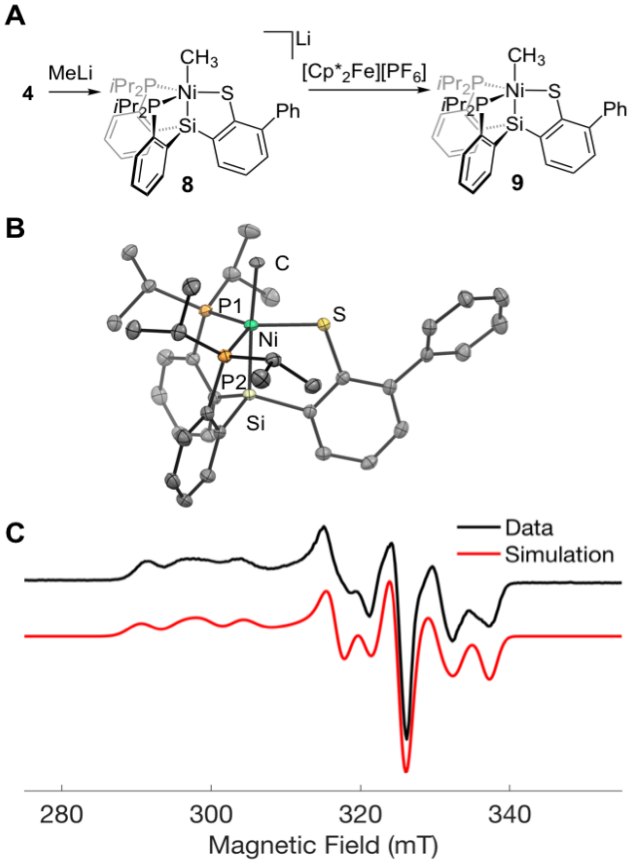

Figure 4. (A) Synthetic route to access compound **9**. (B) X-ray structure of **9**. Hydrogen atoms and disordered components are omitted for clarity. Ellipsoids are depicted at 50% probability. (C) X-band CW EPR spectrum of **9** in 2-MeTHF with simulation. Simulation parameters: **g** = [2.255, 2.073, 2.037]; **A**(^{31}Pα) = [170, 133, 330] MHz; **A**(^{31}Pβ) = [260, 257, 130] MHz.; Acquisition parameters: MW frequency = 9.388 GHz; temperature = 77 K; MW power = 0.5 mW; modulation amplitude = 2 G; conversion time = 82 ms.

Table 2. Bond lengths of **5-H** (DFT) and **9** (XRD).

	***d*(Ni-X)**	***d*(Ni-S)**	***d*(Ni-P)$_{avg}$**	***d*(Ni-Si)**
5-H	1.55	2.22	2.25	2.25
9	2.047(5)	2.1972(6)	2.2428(6)	2.2541(6)

X = H (**5-H**), CH_3 (**9**)

Complex **5-H** could not be obtained in solid-state form due to its highly reactive nature. However, an analogous and more stable Ni^{III}-Me species could be prepared, isolated, and crystallographically characterized. Accordingly, treatment of **4** with methyl lithium yields diamagnetic [(SiP_2S)Ni^{II}Me]Li (**8**), and its oxidation by [Cp*$_2$Fe][PF_6] at −78 °C affords a dark blue-green solu-

tion of $(SiP_2S)Ni^{III}Me$ (**9**, Fig. 4).[35] Structural parameters for **9** compare favorably to the gas-phase, DFT-optimized parameters for **5-H** (Table 2). The 77 K X-band CW EPR spectrum exhibits a rhombic *g* tensor (**g** = [2.255, 2.073, 2.037]) and hyperfine coupling to two similar but distinct ^{31}P nuclei ($\mathbf{A}(^{31}P\alpha)$ = ±[170, 133, 330] MHz; $\mathbf{A}(^{31}P\beta)$ = ±[260, 257, 130] MHz). Compared to that of **5-H**, the EPR spectrum of **9** exhibits slightly greater *g*-anisotropy and comparable $|a_{iso}(^{31}P)|$ values (**5-H**: $|a_{iso}(^{31}P\alpha)| = |a_{iso}(^{31}P\beta)|$ = 223 MHz; **9**: $|a_{iso}(^{31}P\alpha)|$ = 211 MHz, $|a_{iso}(^{31}P\beta)|$ = 216 MHz).

EPR characterization of [(PS_3)NiH][PPN].

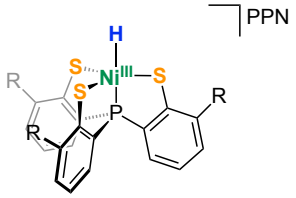

[(PS_3)NiH][PPN]

Figure 5. Structure of **[(PS_3)NiH][PPN]**. R = $SiMe_3$, PPN = $(Ph_3P)_2N^-$

Given the potential value for EPR data of model Ni^{III}-H species to guide reliable assignments of such intermediates in Ni-containing hydrogenases, we also undertook the generation of the previously reported [(PS_3)NiH][PPN] species[17] and the analogous nickel deuteride for related characterization by EPR techniques (Fig. 5). As noted above, previously reported vibrational and EPR data did not locate the presence of the terminal hydride moiety, though its chemical reactivity was consistent with such a formulation.

Through X-band HYSCORE experiments, the ^2H hyperfine coupling for [(PS_3)NiD][PPN] could be detected: $\mathbf{A}(^2H)$ = ±[1.6, 9.3, 9.3] MHz (See Supporting Information for more details). Scaling $\mathbf{A}(^2H)$ by the ratio of the $^1H/^2H$ gyromagnetic ratios ($^1H\gamma/^2H\gamma$= 6.514) approximates a ^1H hyperfine coupling of $\mathbf{A}(^1H)$ = ±[10.4, 60.6, 60.6] MHz in [(PS_3)NiH][PPN], with $|a_{iso}(^1H)|$ = 43.9 MHz and **T** = ±[-33.5, 16.7, 16.7] MHz. The $|a_{iso}(^1H)|$ value corresponds to approximately ±0.03 e- of spin density localized on the hydride of [(PS_3)NiH][PPN], in agreement with a DFT-estimated value of -0.05 e- (gas phase, M06l; see SI). There hence appears to be greater spin delocalization onto the hydride ligand of [(PS_3)NiH][PPN] compared to **5-H**. This difference presumably arises from an increased metal-ligand covalency in **5-H**; a Mulliken spin density of 0.73 e- is calculated on Ni in [(PS_3)NiH][PPN], compared to 0.60 e- in **5-H**.

Comparison of Ni^{III}-H species with the Ni-C hydrogenase state.

In both systems, spin delocalization onto the ligand framework likely stabilizes the Ni^{III}-H species. Consistent with this idea, DFT-calculated Mulliken spin densities (M06-L functional: def2tzvp [Ni] and def2svp [all other atoms] basis sets) suggests that there is considerable spin leakage onto the supporting thiolate ligands of **5-H** (0.22 e-) and [(PS_3)NiH][PPN] (0.07, 0.07, 0.16 e-). For comparison, in the case of the Ni-C hydrogenase state, DFT calculations suggest the presence of significant spin delocalization onto one of the bridging cysteine groups (Fig. 6, BP86 functional),[36] with the majority of spin localized on Ni (0.72 e-) rather than Fe (0.01 e-). Additionally, a spin density of -0.01 e- is calculated on the hydride bridging the Ni and Fe centers; experimental data support $|a_{iso}(^1H)|$ = *ca.* 11 MHz for the hydride ligand in *D. gigas* hydrogenase,[6c] and a value of $|a_{iso}(^1H)|$ = 3.5 MHz is measured for both *Ralstonia eutropha*[6a] and *D. vulgaris* Miyazaki F hydrogenases.[6d]

It has been noted that the $|a_{iso}(^1H)|$ value for the hydride of the Ni-C hydrogenase state is significantly smaller than that anticipated for a hydride covalently bound to Ni,[6a,b,c] given that $|a_{iso}(^1H)|$ for $H\text{-}Ni^{I}(CO)_3$ was reported to be 293 MHz,[15,37] and that of $[H\text{-}Ni(CN)_n]^x$ was estimated to be *ca.* 427 MHz.[16] Assuming these assignments are reliable, one suggested explanation for the discrepancy is the presence of a proximal iron center in the Ni-C state, which may in turn perturb the spin distribution.[6a] However, it has been observed that the spin density on Fe is very low in the Ni-C state,[38] corroborated by DFT calculations.[36] In this context, it is therefore significant that **5-H** and [(PS_3)NiH][PPN] are measured to have $|a_{iso}(^1H)|$ values quite comparable to that of the Ni-C hydride. The data presented here demonstrates that hydrides covalently bound to a paramagnetic Ni center can exhibit comparatively small $|a_{iso}(^1H)|$ values. We attribute the small $|a_{iso}(^1H)|$ of these complexes in part to the significant spin delocalization onto the thiolate ligands of **5-H** and [(PS_3)NiH][PPN], and by extension suggest that the bridging cysteine in the Ni-C state mitigates the magnitude of $|a_{iso}(^1H)|$ in the Ni-C state hydride, likely more so than the proximal Fe center.[39] Furthermore, although DFT-calculated EPR parameters for the hydrogenase structure featuring a bridging hydride between Ni^{III} and Fe^{II} provide a satisfactory fit to experimental data for the Ni-C state,[6f,g] the present study demonstrates that terminally bound Ni^{III} hydrides can bear $|a_{iso}(^1H)|$ values comparable to that measured for the Ni-C state.

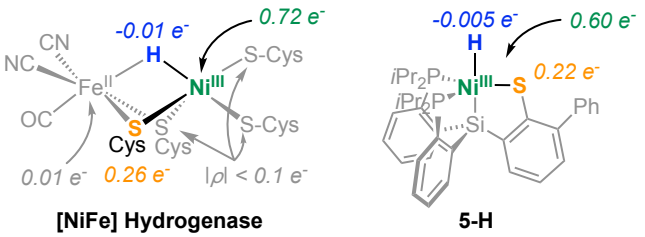

[NiFe] Hydrogenase **5-H**

Figure 6. Calculated Mulliken spin densities of the Ni-C hydrogenase state and **5-H**.

Bimolecular H_2 release from thiolate-Ni^{III}-H and comparison with H_2 release from thiolate-Fe^{III}-H.

Our ability to generate and reliably characterize the Ni^{III}-H species **5-H** enabled us to evaluate its propensity to undergo a bimolecular homocoupling process to generate H_2.[40] Accordingly, dark blue-green solutions of **5-H** prepared *in situ* at −78 °C quantitatively convert to orange solutions of **4** upon warming to 25 °C under N_2. H_2 production was confirmed by GC analysis (98%). The decay of **5-H** to **4** monitored by UV-Vis spectroscopy exhibits isosbestic behavior and is second-order with respect to **5-H** (Fig. 7, k = 20 $M^{-1}\cdot min^{-1}$ at 25 °C). A kinetic isotope effect is observed (k_H/k_D = 1.6 at 25 °C), suggesting that the hydride ligand is present in the rate-determining transition state, and Eyring analysis reveals activation parameters of $\Delta S^{\ddagger}$ = −30(7) cal/(mol·K) and $\Delta H^{\ddagger}$ = 9(2) kcal/mol. The large and negative entropic activation term is consistent with an ordered rate-determining transition state, and these data support the bimolecular reductive elimination of H_2 between two Ni^{III}-H fragments. Metal hydrides with BDFE(M-H) less than half the BDFE of H_2 (BDFE(M-H) < *ca.* 52 kcal/mol in MeCN)[41] are thermodynamically favored to undergo bimolecular reductive elimination of H_2 (2 M-H → 2 M + H_2). Under static vacuum, a THF solution of **5-H** reacts to form the vacant species **6**, which is consistent with the DFT-estimated Ni-H gas-phase BDFE of 57 kcal/mol (**5-H** → $H^{\bullet}$ + **6**).

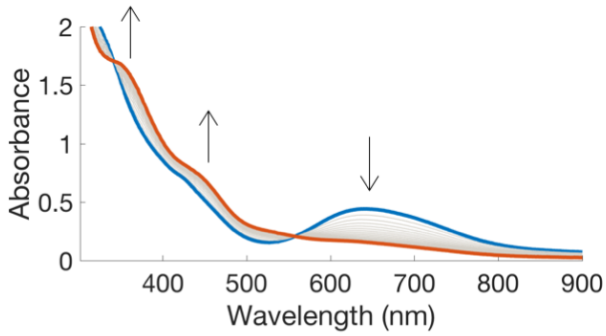

Figure 7. UV-Vis spectra depicting the decay of **5-H** to **4** at 25 °C in THF. Spectra collected in 20 min intervals.

A related S = ½ ferric hydride, $(SiP_2S)Fe^{III}(H)(N_2)$, that we have previously reported,[19] has a DFT-estimated gas phase Fe-H BDFE of 56 kcal/mol ($(SiP_2S)Fe(H)(N_2)$ → $H^{\bullet}$ + $(SiP_2S)Fe(N_2)$) and also undergoes bimolecular reductive elimination of H_2 upon warming to yield the N_2-bridged species $[(SiP_2S)Fe^{II}]_2(N_2)$. Compared to the Ni system, there is a greater degree of spin delocalization onto the hydride ligand in the Fe system, evidenced by a greater $|a_{iso}(^1H)|$ value of 43 MHz. However, HER from the ferric hydride proceeds with a significantly smaller second-order rate constant at 25 °C compared to the Ni system ([Fe]: k = 0.068 $M^{-1}\cdot min^{-1}$, Scheme 2). Additionally, the bimolecular transformation of the ferric hydride bears a large and positive $\Delta S^{\ddagger}$ of 39(13) cal/(mol·K) that we hypothesized to arise from N_2 dissociation prior to H-H bond formation (e.g. {N_2 (*g*) + $[Fe^{III}]$–H···H–$[Fe^{III}(N_2)]$}‡). Such a scenario contrasts with the negative $\Delta S^{\ddagger}$ determined for the present Ni system, which is consistent with an ordered rate-determining transition state (e.g. {$[Ni^{III}]$–H···H–$[Ni^{III}]$}‡).

The unobserved, N_2-dissociated ferric hydride $(SiP_2S)Fe^{III}(H)$ would be an electron-deficient 15 e^- species, favoring N_2 binding to yield a 17 e^- species $(SiP_2S)Fe^{III}(H)(N_2)$. In contrast, the Ni(III) hydride **5-H** is a 17 e^- species, and N_2 binding to form the 19 e^- species $(SiP_2S)Ni^{III}(H)(N_2)$ is thus disfavored. Predissociation of N_2 hence does not play a role in the H_2 evolution chemistry of the Ni system, whereas it does in the Fe system. This is likely a significant factor in the dramatically enhanced rate of H_2 formation in the Ni system compared to Fe. Additionally, because the terminal product is an N_2-bound species, thermodynamic stabilization afforded by N_2 binding may also contribute to the relative rates of H_2 elimination.

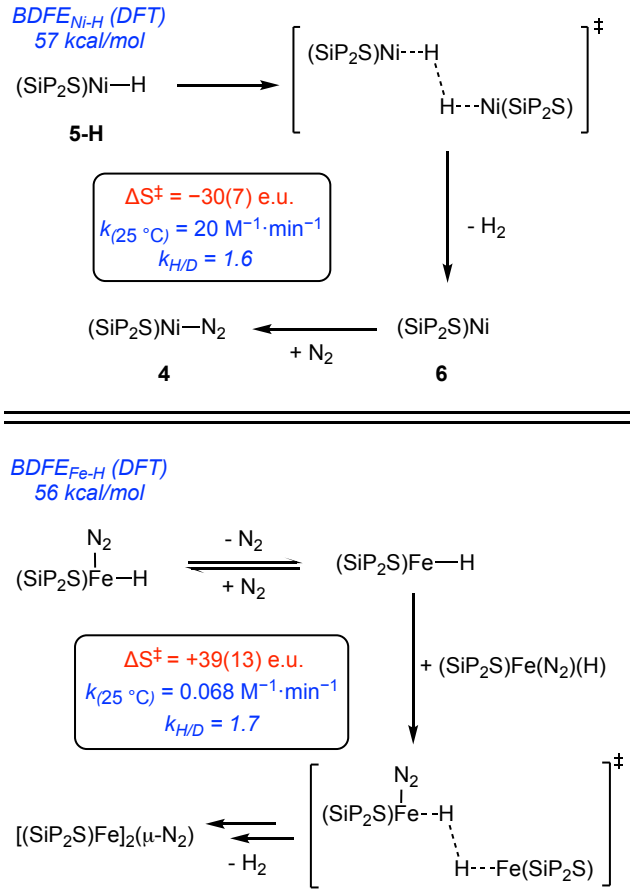

Scheme 2. Comparison of **5-H** and **$(SiP_2S)Fe(H)(N_2)$**, which both undergo bimolecular reductive elimination of H_2 upon warming but with different rates and activation parameters in accord with the presented pathways. Gas-phase BDFEs were calculated with the M06-L functional (def2tzvp [Fe or Ni], def2svp [all other atoms]).

CONCLUSION

In closing, we have reported the synthesis and spectroscopic characterization of an unusual S = ½, terminal Ni^{III}-H species, **5-H**, and its propensity to undergo homolytic bimolecular H-H coupling to release H_2. Heterolytic H_2 evolution via protonation of its 1-electron reduced state, Ni^{II}-H^-, has also been demonstrated. For the Ni^{III}-H of most interest, the sulfur donor bears a considerable amount of spin density (0.22 e^-) based on DFT calculations, stabilizing the system and allowing for the first time direct measurement of salient spectroscopic parameters, including a terminal Ni-H vibration (1728 cm^{-1} in THF) and hyperfine coupling to the terminal hydride ligand ($|a_{iso}(^1H)|$ = 11.7 MHz), as detected via pulse EPR studies. Importantly, this isotropic hyperfine coupling value is similar to that of the hydride ligand in the Ni-C hydrogenase state.[6a,c,d] In contrast, significantly larger $|a_{iso}(^1H)|$ values, on the order of 10^2 MHz, were reported for H-$Ni^I(CO)_4$[15] and [H-$Ni(CN)_n$]^x [16] (via generation and detection in a solid matrix), the only previous examples of terminal Ni-H species with reported $|a_{iso}(^1H)|$ values.

The discrepancy between the significantly smaller $|a_{iso}(^1H)|$ measured for the assigned Ni-*H*-Fe moiety of the Ni-C hydrogenase state, compared to previously reported paramagnetic nickel hydride species, has been highlighted previously.[6a,b,c] The EPR data for the well-defined Ni^{III}-H species featured herein demonstrates that smaller $|a_{iso}(^1H)|$ values are compatible with a nickel hydride ligand assignment, especially when covalently bound to a spin active nickel center with one (or more) sulfur donors, as is suggested for the Ni-C hydrogenase state. Thus, the Ni^{III}-H species reported here, as well as related structures in future studies, can provide valuable platforms for constraining spectroscopic assignments in enzymatic systems and identifying specific reactivity patterns, including H-H bond formation to generate H_2.

ASSOCIATED CONTENT

Supporting Information

The Supporting Information is available free of charge on the ACS Publications website at **http://pubs.acs.org**.

Experimental procedures and compound characterization data (PDF)

X-ray data (CIF)

AUTHOR INFORMATION

Corresponding Author

jpeters@caltech.edu

ORCID

Nina X. Gu: 0000-0002-4637-8418
Paul H. Oyala: 0000-0002-8761-4667
Jonas C. Peters: 0000-0002-6610-4414

Notes

The authors declare no competing financial interests.

ACKNOWLEDGMENTS

The authors acknowledge Gerri Roberts for preliminary data, and Dr. Michael Takase and Lawrence Henling for assistance with X-ray crystallography. This work was supported by the Department of Energy (DOE-0235032) and NSF-GRFP (N.X.G.). The Caltech EPR facility was supported by the NSF (NSF-1531940) and the Dow Next Generation Educator Fund. The X-Ray Crystallography Facility in the Beckman Institute at Caltech was supported by the Dow Next Generation Instrumentation Grant.

REFERENCES

[1] (a) McKone, J. R.; Marinescu, S. C.; Brunschwig, B. S.; Winkler, J. R.; Gray, H. B. Earth-Abundant Hydrogen Evolution Electrocatalysts. *Chem. Sci.* **2014**, *5*, 865-878. (b) Bullock, R. M.; Appel, A. M.; Helm, M. L. Production of Hydrogen By Electrocatalysis: Making the H-H Bond by Combining Protons and Hydrides. *Chem. Commun.* **2014**, *50*, 3125-3143. (c) Tong, L.; Duan, L.; Zhou, A.; Thummel, R. P. First-row transition metal polypyridine complexes that catalyze proton to hydrogen reduction. *Coord. Chem. Rev.* **2020**, *402*, 213097. (d) Artero, V.; Chavarot-Kerlidou, M.; Fontecave, M. Splitting Water with Cobalt. *Angew. Chem. Int. Ed.* **2011**, *50*, 7238-7266.

[2] (a) Haddad, A. Z.; Garabato, B. D.; Kozlowski, P. M.; Buchanan, R. M.; Grapperhaus, C. A. Beyond Metal-Hydrides: Non-Transition-Metal and Metal-Free Ligand-Centered Electrocatalytic Hydrogen Evolution and Hydrogen Oxidation. *J. Am. Chem. Soc.* **2016**, *138*, 7844-7847. (b) Thompson, E. J.; Berben, L. A. Electrocatalytic Hydrogen Production by an Aluminum(III) Complex: Ligand-Based Proton and Electron Transfer. *Angew. Chem. Int. Ed.* **2015**, *54*, 11642-11646.

[3] (a) James, T. L.; Cai, L.; Muetterties, M. C.; Holm, R. C. Dihydrogen evolution by protonation reactions of nickel(I). *Inorg. Chem.* **1996**, *35*, 4148-4161. (b) Lahiri, G. K.; Schussel, L. J.; Stolzenberg, A. M. F430 model chemistry. Mechanistic investigation of the reduction, coupling, and dehydrohalogenation of alkyl halides by the Nickel(I) Octaethylisobacteriochlorin Anion. *Inorg. Chem.* **1992**, *31*, 4991-5000.

[4] (a) Efros, L. L.; Thorp, H. H.; Brudvig, G. W.; Crabtree, R. H. Towards a Functional Model of Hydrogenase: Electrocatalytic Reduction of Protons to Dihydrogen by a Nickel Macrocylic Complex. *Inorg. Chem.* **1992**, *31*, 1722-1724. (b) Beley, M.; Collin, J.-P.; Ruppert, R.; Sauvage, J.-P. Electrocatalytic reduction of carbon dioxide by nickel cyclam2+ in water: study of the factors affecting the efficiency and the selectivity of the process. *J. Am. Chem. Soc.* **1986**, *108*, 7461-7467. (c) Collin, J.-P.; Jouaiti, A.; Sauvage, J.-P. Electrocatalytic Properties of $Ni(cyclam)^{2+}$ and $Ni_2(biscyclam)^{4+}$ with Respect to CO_2 and H_2O Reduction. *Inorg. Chem.* **1988**, *27*, 1986-1990. (d) Kaur-Ghumaan, S.; Hasche, P.; Spannenberg, A.; Beweries, T. Nickel(II) PE^1CE^2P pincer complexes (E = O, S) for electrocatlytic proton reduction. *Dalton Trans.* **2019**, *48*, 16322-16329. (e) Luca, O. R.; Blakemore, J. D.; Konezny, S. J.; Praetorius, J. M.; Schmeier, T. J.; Hunsinger, G. B.; Batista, V. S.; Brudvig, G. W.; Hazari, N.; Crabtree, R. H. Organometallic Ni Pincer Complexes for the Electrocatalytic Production of Hydrogen. *Inorg. Chem.* **2012**, *51*, 8704-8709. (f) Han, Y.; Fang, H.; Jing, H.; Sun, H.; Lei, H.; Lai, W.; Cao, R. Singly versus Doubly Reduced Nickel Porphyrins for Proton Reduction: Experimental and Theoretical Evidence for a Homolytic Hydrogen-Evolution Reaction. *Angew. Chem. Int. Ed.* **2016**, *55*, 5457-5462.

[5] Additionally, paramagnetic $Ni^{I/III}$ hydrides have been proposed as intermediates in catalytic organometallic transformations, see: (a) Kuang, Y.; Anthony, D.; Katigbak, J.; Marrucci, F.; Humagain, S.; Diao, T. Ni(I)-Catalyzed Reductive Cyclization of 1,6-Dienes: Mechanism-Controlled *trans* Selectivity. *Chem* **2017**, *3*, 268-280. (b) Zarate, C.; Yang, H.; Bezdek, M. J.; Hesk, D.; Chirik, P. J. Ni(I)-X Complexes Bearing a Bulky α-Diimine Ligand Synthesis, Structure, and

Superior Catalytic Performance in the Hydrogen Isotope E xchange in Pharmaceuticals. *J. Am. Chem. Soc.* **2019**, *141*, 5034-5044.

[6] (a) Brecht, M.; van Gastel, M.; Buhrke, T.; Friedrich, B.; Lubitz, W. Direct Detection of a Hydrogen Ligand in the [NiFe] Center of the Regulatory H_2-Sensing Hydrogenase from *Ralstonia Eutropha* in its Reduced State by HYSCORE and ENDOR Spectroscopy. *J. Am. Chem. Soc.* **2003**, *125*, 13075-13083. (b) Whitehead, J. P.; Gurbiel, R. J.; Bagyinka, C.; Hoffman, B. M.; Maroney, M. J. The Hydrogen Binding Site in Hydrogenase: 35-GHz ENDOR and XAS Studies of the Ni-C Active Form and the Ni-L Photoproduct. *J. Am. Chem. Soc.* **1993**, *115*, 5629-5635. (c) Fan, C.; Teixeira, M.; Moura, J.; Moura, I.; Hanh, H. B.; Le Gall, J.; Peck, H. D.; Hoffman, B. M. Detection and characterization of exchangeable protons bound to the hydrogen-activation nickel site of *Desulfovibrio gigas* hydrogenase: a proton and deuterium Q-band ENDOR study. *J. Am. Chem. Soc.* **1991**, *113*, 20-24. (d) Foerster, S; van Gastel, M.; Brecht, M.; Lubtiz, W. An orientation-selected ENDOR and HYSCORE study of the Ni-C active state of *Desulfovibrio vulgaris* Miyazaki F hydrogenase *J. Biol. Inorg. Chem.* **2005**, *10*, 51-62. (e) Lubitz, W.; Ogata, H.; Rüdiger, O.; Reijerse, E. Hydrogenases. *Chem. Rev.* **2014**, *114*, 4081-4148. (f) Foerster, S.; Stein, M.; Brecht, M.; Ogata, H.; Higuchi, Y.; Lubitz, W. Single Crystal EPR Studies of the Reduced Active Site of [NiFe] Hydrogenase from *Desulfovibrio vulgaris* Miyazaki F. *J. Am. Chem. Soc.* **2003**, *125*, 83-93. (g) Stein, M.; van Lenthe, E.; Jan Baerends, E.; Lubitz, W. Relativistic DFT Calculations of the Paramagnetic Intermediates of [NiFe] Hydrogenase. Implications for the Enyzmatic Mechanism. *J. Am. Chem. Soc.* **2001**, *123*, 5839-5840.

[7] Stein, M.; Lubitz, W. The electronic structure of the catalytic intermediate Ni-C in [NiFe] and [NiFeSe] hydrogenases. *Phys. Chem. Chem. Phys.* **2001**, *3*, 5115-5120.

[8] In the EPR-silent Ni-R state (Ni^{II}-H-Fe^{II}), XRD and NRVS data suggest that the hydride is also bound more tightly to Ni than Fe. See: (a) Ogata, H.; Nishikawa, K.. Lubitz, W. Hydrogens detected by subatomic resolution protein crystallography in [NiFe] hydrogenase. *Nature* **2015**, *520*, 571-574. (b) Ogata, H.; Krämer, T.; Wang, H.; Schilter, D.; Pelmenschikov, V.; van Gastel, M.; Neese, F.; Rauchfuss, T. B.; Gee, L. B.; Scott, A. D.; Yoda, Y.; Tanaka, Y.; Lubitz, W.; Cramer, S. P. Hydride bridge in [NiFe]-hydrogenase observed by nuclear resonance vibrational spectroscopy. *Nat. Commun.* **2015**, *6*, 7890.

[9] Nilsson Lill, S. O.; Siegbahn, P. E. M. An Autocatalytic Mechanism for NiFe-Hydrogenase: Reduction to Ni(I) Followed by Oxidative Addition. *Biochemistry* **2009**, *48*, 1056-1066.

[10] (a) Slater, J. W.; Marguet, S. C.; Monaco, H. A.; Shafaat, H. S. Going beyond Structure: Nickel-Substituted Rubredoxin as a Mechanistic Model for the [NiFe] Hydrogenases. *J. Am. Chem. Soc.* **2018**, *140*, 10250-10262. (b) Slater, J. W.; Marguet, S. C.; Cirino, S. L.; Maugeri, P. T.; Shafaat, H. S. Experimental and DFT Investigations Reveal the Influence of the Outer Coordinate Sphere on the Vibrational Spectra of Nickel-Substituted Rubredoxin, A Model Hydrogenase Enzyme. *Inorg. Chem.* **2017**, *56*, 3926-3938.

[11] (a) Lee, C.-M.; Chen, C.-H.; Liao, F.-X.; Hu, C.-H.; Lee, G.-H. Mononuclear Ni^{III}-Alkyl Complexes (Alkyl = Me and Et): Relevance to the Acetyl-CoA Synthase and Methyl-CoM Reductase. *J. Am. Chem. Soc.* **2010**, *132*, 9256-9258. (b) Zheng, B.; Tang, F.; Luo, J.; Schultz, J. W.; Rath, N. P.; Mirica, L. M. Organometallic Nickel(III) Complexes Relevant to Cross-Coupling and Carbon-Heteroatom Bond Formation Reactions. *J. Am. Chem. Soc.* **2014**, *136*, 6499-6504. (c) Lipschutz, M. I.; Yang, X.; Chatterjee, R.; Tilley, T. D. A Structurally Rigid Bis(amido) Ligand Framework in Low-Coordinate Ni(I), Ni(II), and Ni(III) Analogues Provides Access to a Ni(III) Methyl Complex via Oxidative Addition. *J. Am. Chem. Soc.* **2013**, *135*, 15298-15301. (d) Schultz, J. W.; Fuchigami, K.; Zheng, B.; Rath, N. P.; Mirica, L. M. Isolated Organometallic Nickel(III) and Nickel(IV) Complexes Relevant to Carbon-Carbon Bond Formation Reactions. *J. Am. Chem. Soc.* **2016**, *138*, 12928-12934. (e) Diccianni, J. B.; Hu, C. T.; Diao, T. (Xantphos)Ni(I)-Alkyl Mediated Insertion of CO_2. *Angew. Chem. Int. Ed.* **2019**, *58*, 13865-13868.

[12] (a) Dong, Q.; Zhao, Y.; Su, Y.; Su, J.-H.; Wu, B.; Yang, X.-J. Synthesis and Reactivity of Nickel Hydride Complexes of a α-Diimine Ligand. *Inorg. Chem.* **2012**, *51*, 13162-13170. (b) Kriley, C. E.; Woolley, C. J.; Krepps, M. K.; Popa, E. M.; Fanwick, P. E.; Rothwell, I. P. Synthesis and Characterization of a Series of Novel Nickel(II):Nickel(I) Complexes. Crystal Structures of $[NiCl_2(dcpm)]$, $[Ni(dcpm)_2](NO_3)_2{\cdot}2EtOH$, $[Ni_2Cl_2(\mu\text{-}dcpm)_2(\mu\text{-}H)]$ and $[Ni_2(\mu\text{-}PCy_2)_2(PCy_2Me)_2]$; dcpm-bis(dicyclohexylphosphino)methane *Inorg. Chim. Acta.* **2000**, *300-302*, 200-205. (c) Pfirrmann, S.; Limberg, C.; Herwig, C.; Knispel, C.; Braun, B.; Bill, E.; Stösser, R. A Reduced β-Diketiminato-Ligated Ni_3H_4 Unit Catalyzing H/D Exchange. *J. Am. Chem. Soc.* **2010**, *132*, 13684-13691. (d) Beck, R.; Shoshani, M.; Johnson, S. A. Catalytic Hydrogen/Deuterium Exchange of Unactivated Carbon-Hydrogen Bonds by a Pentanuclear Electron-Deficient Nickel Hydride Cluster. *Angew. Chemie. Int. Ed.* **2012**, *51*, 11753-11756. (e) Gehring, H.; Metzinger, R.; Herwig, C.; Intemann, J.; Harder, S.; Limberg, C. Hydride Reactivity of Ni^{II}-X-Ni^{II} Entities: Mixed-Valent Hydrido Complexes and Reversible Metal Reduction. *Chem. Eur. J.* **2013**, *19*, 1629-1636. (f) Yao, S. A.; Corcos, A. R.; Infante, I.; Hillard, E. A.; Clérac, R.; Berry, J. F. An "Intermediate Spin" Nickel Hydride Complex Stemming from Delocalized $Ni_2(\mu\text{-}H)_2$ Bonding. *J. Am. Chem. Soc.* **2014**, *136*, 13538-13541. (g) Ogo, S.; Kabe, R.; Uehara, K.; Kure, B.; Nishimura, T.; Menon, S. C.; Harada, R.; Fukuzumi, S.; Higuchi, Y.; Ohhara, T.; Tamada, T.; Kuroki, R. A Dinuclear Ni(μ-H)Ru Complex Derived from H_2 *Science* **2007**, *316*, 585-587.

[13] (a) Müller, J.; Dorner, H.; Huttner, G.; Lorenz, H. Tetrakis(η-cyclopentadienyl)tetranickel Trihydride-An Unusual Tetranuclear Cluster. *Angew. Chemie. Int. Ed.* **1973**, *12*, 1005-1006. (b) Smith, M. E.; Andersen, R. A. Preparation of the Paramagnetic Hydrides $(Me_5C_5)_3M_3(\mu_3\text{-}CH)(\mu\text{-}H)$ (M = Ni, Co). *Organometallics* **1996**, *15,* 2680-2682.

[14] (a) Kandiah, M.; McGrady, G. S.; Decken, A.; Sirsch, P. [(Triphos)Ni(η^2-BH_4)]: An Unusual Nickel(I) Borohydride Complex. *Inorg. Chem.* **2005**, *44*, 8650-8652. (b) Journaux, Y.; Lozan, V.; Klingele, J.; Kersting, B. Stabilisation of a Paramagnetic BH_4^- bridged Dinickel(II) Complex by a Macrodinucleating Hexaazadithiophenolate Ligand. *Chem. Commun.* **2006**, 83-84. (c) MacMillan, S. N. Ph.D. Dissertation, Boron in the Primary and Secondary Coordination Spheres of Iron and Nickel. Massachusetts Institute of Technology, Cambridge, MA, 2013.

[15] The authors favor the assignment as a trigonal pyramidal H-$Ni(CO)_3$ species, but also note that H-$Ni(CO)_x$ ($x \geq 2$) could not be experimentally ruled out as possible assignments, see: Morton, J. R.; Preston, K. F. An ESR study at 4 K of the reaction between H and $Ni(CO)_4$. *J. Chem. Phys.* **1984**, *81*, 5775-5778.

[16] Irradiation of $Ni(CN)_4^{2-}$ in the presence of water results in the generation of several EPR-active species. One of the species exhibits a large $|a_{iso}(^1H)|$ value of *ca.* 427 MHz and an axial g tensor (**g** = [2.00, 2.05, 2.05]), which was initially attributed to H-$Ni^{III}(CN)_4^{2-}$ (See: Symons, M. C. R.; Aly, M. M.; West, D. X. Electron spin resonance data for the hydrogen-transition metal bond in the complex $[HNi(CN)_4]^{2-}$ *J. Chem. Soc., Chem. Commun.* **1979**, 51-52). However, the subsequent study of H-$Ni^{I}(CO)_3$ revealed similar EPR parameters to that of the putative H-$Ni^{III}(CN)_4^{2-}$ complex, and the authors suggest that H-$Ni^{I}(CN)_3^{3-}$ is also a plausible assignment given the available data (See Ref. 15).

[17] Lai, K.-T.; Ho, W.-C.; Chiou, T.-W.; Liaw, W.-F. Formation of $[Ni^{III}(\kappa^1\text{-}S_2CH)(P(o\text{-}C_6H_3\text{-}3\text{-}SiMe_3\text{-}2\text{-}S)_3)]^-$ via CS_2 Insertion into Nickel(III) Hydride Containing $[Ni^{III}(H)(P(o\text{-}C_6H_3\text{-}3\text{-}SiMe_3\text{-}2\text{-}S)_3)]^-$. *Inorg. Chem.* **2013**, *52*, 4151-4153.

[18] In Ref. 17, it is noted that H_2 and $[Ni_2^{II}(P(C_6H_3\text{-}3\text{-}SiMe_3\text{-}2\text{-}S)_3)_2]^{2-}$ are detected upon warming a solution of $[(PS_3)NiH][PPN]$. However, because the yields of either product are not included, it is not clear whether H_2 loss is a major reaction pathway.

[19] Gu, N. X.; Oyala, P. H.; Peters, J. C. An S = ½ Iron Complex Featuring N_2, Thiolate, and Hydride Ligands: Reductive Elimination of H_2 and Relevant Thermochemical Fe-H Parameters. *J. Am. Chem. Soc.* **2018,** *140*, 6374-6382.

[20] Suess, D. L. M.; Tsay, C.; Peters, J. C. Dihydrogen Binding to Isostructural $S = ½$ and $S = 0$ Cobalt Complexes. *J. Am. Chem. Soc.* **2012**, *134*, 14158-14164.
[21] Crabtree, R. H. Dihydrogen Complexation. *Chem. Rev.* **2016**, *116*, 8750-8769.
[22] (a) Tsay, C.; Peters, J. C. Thermally Stable N_2 and H_2 Adducts of Cationic Nickel(II) *Chem. Sci*. **2012**, *3*, 1313-1318. (b) Connelly, S. J.; Zimmerman, A. C.; Kaminsky, W.; Heinekey, D. M. Synthesis, Structure, and Reactivity of a Nickel Dihydrogen Complex. *Chem. Eur. J.* **2012**, *18*, 15932-15934. (c) He, T.; Tsvetkov, N. P.; Andino, J. G.; Gao, X.; Fullmer, B. C.; Caulton, K. G. Mechanism of Heterolysis of H_2 by an Unstaturated d^8 Nickel Center: via Tetravalent Nickel? *J. Am. Chem. Soc.* **2010**, *132*, 910-911. (d) Sweany, R. L.; Polito, M. A.; Moroz, A. Photolysis of Tetracarbonylnickel in Dihydrogen-containing Matrixes. Evidence for the Formation of a Complex of Molecular Hydrogen. *Organometallics* **1989**, *8*, 2305-2308.
[23] For examples of d^{10} Ni(H_2) complexes supported by group 13 Z-type ligands, see: (a) Cammarota, R. C.; Lu, C. C. Tuning Nickel with Lewis Acidic Group 13 Metalloligands for Catalytic Olefin Hydrogenation. *J. Am. Chem. Soc.* **2015**, *137*, 12486-12489. (b) Harman, W. H.; Lin, T.-P.; Peters, J. C. A d^{10} Ni-(H_2) Adduct as an Intermediate in H-H Oxidative Addition across a Ni-B Bond. *Angew. Chem. Int. Ed.* **2014**, *53*, 1081-1086.
[24] (a) Olechnowicz, F.; Hillhouse, G. L.; Cundari, T. R.; Jordan, R. F. Heterolytic H-H and H-B Bond Cleavage Reactions of {(IPr)Ni(μ-S)}$_2$. *Inorg. Chem*. **2017**, *56*, 9922-9930. (b) Sellmann, D.; Geipel, F.; Moll, M. [Ni(NHP*n*Pr$_3$)('S_3')], the First Nickel Thiolate Complex Modeling the Nickel Cysteinate Site and Reactivity of [NiFe] Hydrogenase. *Angew. Chem. Int. Ed.* **2000**, *39*, 561-563.
[25] Bulk electrolysis experiments confirmed the generation of 5.8 ± 0.6 equivalents of H_2 per Ni center (106 ± 5% FE) over 4 hours in THF at a controlled potential of -2.7 V vs. Cp_2Fe/Cp_2Fe^+. The yield of H_2 is the average of two independent runs. Only trace H_2 is detected in the absence of PhOH. In the absence of **4**, there is a small but measurable background HER process accounting for 0.6 equiv H_2, corrected for in the yield of the Ni-catalyzed process. Rinse test experiments were consistent with a molecular catalyst but do not reliably rule out a heterogeneous component.
[26] Besora, M.; Lledos, A.; Maseras, F. Protonation of Transition-Metal Hydrides: A Not so Simple Process. *Chem. Soc. Rev.* **2009**, *38*, 957−966.
[27] For examples of bimolecular HER from first-row transition metal hydrides, see: (a) Halpern, J.; Pribanić Hydrogenase of Pentacyanocobaltate(II) at High Pressures. *Inorg. Chem*. **1970**, *9*, 2616-2618. (b) Ungváry, F.; Markó, L. Kinetics and Mechanism of the Decomposition of Cobalt Tetracarbonyl Hydride to Dicobalt Octacarbonyl and Hydrogen. *J. Organomet. Chem.* **1969**, *20*, 205-209. (c) Prokopchuk, D. E.; Chambers, G. M.; Walter, E. D.; Mock, M. T.; Bullock, R. M. H_2 Binding, Splitting, and Net Hydrogen Atom Transfer at a Paramagnetic Iron Complex. *J. Am. Chem. Soc.* **2019**, *141*, 1871-1876. (d) Rettenmeier, C.; Wadepohl, H.; Gade, L. H. Stereoselective Hydrodehalogenation via a Radical-Based Mechanism Involving T-Shaped Chiral Nickel(I) Pincer Complexes. *Chem. Eur. J.* **2014**, *20*, 9657-9665. (e) Marinescu, S. C.; Winkler, J. R.; Gray, H. B. Molecular Mechanisms of Cobalt-Catalyzed Hydrogen Evolution. *Proc. Natl. Acad. Sci.* **2012**, *109*, 15127-15131. (f) Kuo, J. L.; Gunasekara, T.; Hansen, A.; Vibbert, H. B.; Bohle, F.; Norton, J. R.; Grimme, S.; Guinlivan, P. J. Thermodynamics of $H^+/H^•/H^-/e^-$ Transfer from $[CpV(CO)_3H]^-$: Comparisons to the Isoelectronic $CpCr(CO)_3H$. *Organometallics* **2019**, *38*, 4319-4328.
[28] For examples of bimolecular HER from 2nd and 3rd row transition metal hydrides, see: (a) Collman, J. P.; Wagenknecht, P. S.; Lewis, N. S. Hydride Transfer and Dihydrogen Elimination from Osmium and Ruthenium Metalloporphyrin Hydrides: Model Processes for Hydrogenase Enzymes and the Hydrogen Electrode Reaction. *J. Am. Chem. Soc.* **1992**, *114*, 5665−5673. (b) Collman, J. P.; Hutchison, J. E.; Wagenknecht, P. S.; Lewis, N. S.; Lopez, M. A.; Guilard, R. An Unprecedented, Bridged Dihydrogen Complex of a Cofacial metallodiporphyrin and its Relevance to the Bimolecular Reductive Elimination of Hydrogen. *J. Am. Chem. Soc.* **1990**, *112*, 8206−8208. (c) Norton, J. R. Organometallic Elimination Mechanisms: Studies on Osmium Alkyls and Hydrides. *Acc. Chem. Res.* **1979**, *12*, 139−145. (d) Evans, J.; Norton, J. R. Mechanism of Reductive Elimination. I. Dinuclear Elimination of Hydrogen from Cis-dihydridotetracarbonylosmium. *J. Am. Chem. Soc.* **1974**, *96*, 7577−7578. (e) Inoki, D.; Matsumoto, T.; Nakai, H.; Ogo, S. Experimental Study of Reductive Elimination of H_2 from Rhodium Hydride Species. *Organometallics* **2012**, *31*, 2996−3001.
[29] For an example of unimolecular H_2 evolution from a dinickel(II) dihydride species, see: Manz, D.-H.; Duan, P.-C.; Dechert, S.; Demeshko, S.; Oswald, R.; John, M.; Mata, R. A.; Meyer, F. *J. Am. Chem. Soc.* **2017**, *139*, 16720-16731.
[30] (a) Hu, X.; Brunschwig, B. S.; Peters, J. C. Electrocatalytic Hydrogen Evolution at Low Overpotentials by Cobalt Macrocyclic Glyoxime and Tetraimine Complexes. *J. Am. Chem. Soc.* **2007**, *129*, 8988-8998. (b) Rose, M. J.; Gray, H. B.; Winkler, J. R. Hydrogen Generation Catalyzed by Fluorinated Digyloxime-Iron Complexes at Low Overpotentials. *J. Am. Chem. Soc.* **2012**, *134*, 8310-8313.
[31] Based on the harmonic oscillator model, the Ni-D stretch of **5-D** is estimated to be 1232 cm^{-1}. This falls in a region that is dominated by intense IR stretches from THF, and the Ni-D stretch could not be resolved in the solution IR spectrum collected in THF at -78 °C. (See Figs. S40, S41).
[32] The gas-phase DFT calculated Ni-H stretches for **2** (calc: 1742 cm^{-1}, expt: 1737 cm^{-1}) and **3** (calc: 1689 cm^{-1}, expt: 1677 cm^{-1}) are also in good agreement with the experimental solid-state IR stretches. (M06-L functional: def2tzvp [Ni], def2svp [all other atoms])
[33] (a) Kinney, R. A.; Saouma, C. T.; Peters, J. C.; Hoffman, B. M. Modeling the Signatures of Hydrides in Metalloenzymes: ENDOR Analysis of a Di-iron Fe(μ-NH)(μ-H)Fe Core. *J. Am. Chem. Soc.* **2012**, 134, 12637-12647. (b) Hoeke, V.; Tociu, L.; Case, D. A.; Seefeldt, L. C.; Raugei, S.; Hoffman, B. M. High-Resolution ENDOR Spectroscopy Combined with Quantum Chemical Calculations Reveals the Structure of Nitrogenase Janus Intermediate E_4(4H). *J. Am. Chem. Soc.* **2019**, *141*, 11984-11996.
[34] Wittke, J. P.; Dicke, R. H. Redetermination of the Hyperfine Splitting in the Ground State of Atomic Hydrogen. *Phys. Rev.* **1956**, *103*, 620−631.
[35] The apical ligand of compound **9** is modeled with 87% occupancy as Ni-CH_3 and 13% occupancy as Ni-N_2. The presence of the disordered component results from the slow decomposition of **9** in solution at -35 °C.
[36] Kampa, M.; Lubitz, W.; van Gastel, M.; Neese, F. Computation study of the electronic structure and magnetic properties of the Ni-C state in [NiFe] hydrogenases including the second coordination sphere. *J. Biol. Inorg. Chem.* **2012**, *17*, 1269-1281.
[37] Stein, M.; van Lenthe, E.; Baerends, E. J.; Lubitz, W. g- and A-Tensor Calculations in the Zero-Order Approximation for Relativistic Effects of Ni Complexes $Ni(mnt)_2^-$ and $Ni(CO)_3H$ as Model Complexes for the Active Center of [NiFe]-Hydrogenase. *J. Phys. Chem. A.* **2001**, *105*, 416-425.
[38] Huyett, J. E.; Carepo, M.; Pamplona, A.; Franco, R.; Moura, I.; Moura, J. J. G.; Hoffman, B. M. ^{57}Fe Q-Band Pulsed ENDOR of the Hetero-Dinuclear Site of Nickel Hydrogenase: Comparison of the NiA, NiB, and NiC States. *J. Am. Chem. Soc.* **1997**, *119*, 9291-9292.
[39] Another proposed cause for the small ^{1}H hyperfine coupling of the Ni-C state is that the hydride resides close to the equatorial plane (near the nodal surface) of the singly-populated Ni(d_{z^2}) orbital of a distorted square pyramidal Ni center, where three cysteines and the hydride lie approximately along the xy-plane (See Refs. 6a,d,e and 37). For comparison, the DFT-optimized structure of **5-H** is best described as a distorted trigonal bipyramid. Nonetheless, a $S = ½$, d^7 configuration for a trigonal bipyramidal complex would place the unpaired electron largely in xy-plane (defining the z-axis along the C_3-axis). The combination of significant spin delocalization onto the thiolate and limited spatial overlap with the singly-occupied Ni d orbital in the xy-plane likely both contribute to the small $a_{iso}(^1H)$ value for **5-H**. These are analogous factors to what is hypothesized for

the Ni-C hydrogenase state, which is measured to have a hydride $|a_{iso}(^1H)|$ value of comparable magnitude as **5-H**.

[40] Related H• transfer from a Ni(II)-H species has been previously demonstrated, see: (a) Ref. 27d (b) Yao, C.; Wang, S.; Norton, J. R.; Hammond, M. Catalyzing the Hydrodefluorination of CF_3-substituted Alkenes by $PhSiH_3$. H• Transfer from a Nickel Hydride. *J. Am. Chem. Soc.* **2020**, *142*, 4793-4799.

[41] Wiedner, E. S.; Chambers, M. B.; Pitman, C. L.; Bullock, R. M.; Miller, A. J. M.; Appel, A. M. Thermodynamic Hydricity of Transition Metal Hydrides. *Chem. Rev.* **2016**, *116*, 8655-8692.

TOC Graphic